33rd Annual International Conference of the IEEE EMBS
Boston, Massachusetts USA, August 30 - September 3, 2011

Target Motion Predictions for Pre-operative Planning during Needle-Based Interventions

Jorn op den Buijs, Momen Abayazid, Chris L. de Korte, and Sarthak Misra

Abstract— **During biopsies, breast tissue is subjected to displacement upon needle indentation, puncture, and penetration. Thus, accurate needle placement requires pre-operative predictions of the target motions. In this paper, we used ultrasound elastography measurements to non-invasively predict elastic properties of breast tissue phantoms. These properties were used in finite element (FE) models of indentation of breast soft tissue phantoms. To validate the model predictions of target motion, experimental measurements were carried out. Breast tissue phantoms with cubic and hemispherical geometries were manufactured and included materials with different elastic properties to represent skin, adipose tissue, and lesions. Ultrasound was used to track the displacement of the target (i.e., the simulated lesion) during indentation. The FE model predictions were compared with ultrasound measurements for cases with different boundary conditions and phantom geometry. Maximum errors between measured and predicted target motions were 12% and 3% for the fully supported and partially supported cubic phantoms at 6.0 mm indentation, respectively. Further, FE-based parameter sensitivity analysis indicated that increasing skin elastic modulus and reducing the target depth location increased the target motion. Our results indicate that with *a priori* knowledge about the geometry, boundary conditions, and linear elastic properties, indentation of breast tissue phantoms can be accurately predicted with FE models. FE models for pre-operative planning in combination with robotic needle insertions, could play a key role in improving lesion targeting for breast biopsies.**

I. Introduction

In the United States, breast cancer kills 40,000 women each year, and more than 200,000 women were diagnosed with the disease in 2010 [1]. Early detection and diagnosis is of key importance for the effective treatment of breast cancer. Insertion of a needle into soft tissue is frequently used to take samples from a breast lump that is visible on a mammogram or ultrasound. These samples will be screened for malignancy. During needle insertion, the clinician may use medical imaging (e.g., ultrasound or magnetic resonance imaging) to target the suspected tumor [2], [3], [4]. Accurate needle placement is important for a correct diagnosis, especially since the size of detected lumps is decreasing with increased diagnostic performance. During indentation, puncture and penetration of the needle, target motion occurs [5] (Figure 1), which may result in needle misplacements. Target displacements of over 2.0 mm have been measured during placement of a biopsy needle in the breast [6].

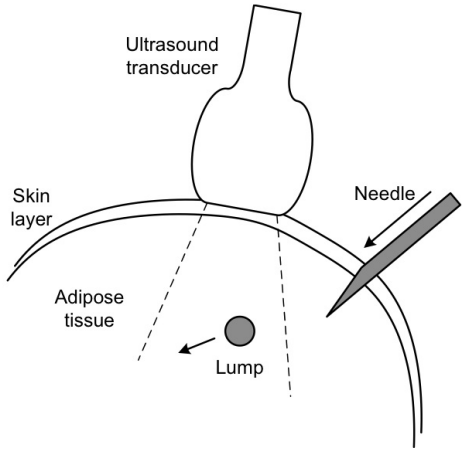

Fig. 1. Schematic of an ultrasound-guided breast biopsy: Compression by the ultrasound transducer, as well as interactions between needle and soft tissue cause target motion.

The targeting accuracy of the needle could potentially be increased by using precisely controllable robotic needle insertion devices [7], [8], which use pre-operative planners based on detailed, patient-specific models of needle-tissue interaction [9], [10]. To model needle insertion, its different phases need to be described. Needle insertion can be divided into indentation, puncture, and penetration [11]. The needle is initially in contact with the surface (skin layer) of the breast tissue. Upon forward displacement of the needle, it indents the tissue surface which becomes deformed. After reaching an energy threshold, the tissue ruptures at the needle tip and a crack is initiated. After puncture, the deformation of the tissue surface relaxes and the needle penetrates further into the tissue. During insertion, friction acts between needle and tissue. Since tissue surface indentation is a major cause of target motion [12], accurate predictions of target motion upon breast tissue indentation are important for the guidance of robotic devices for needle insertions during needle-based interventions, such as biopsies, interstitial brachytherapy, or radiofrequency ablation.

Predictions of target motion could be made by modeling soft tissue deformation and surgical tool-tissue interactions with the finite element (FE) method [9]. FE models require knowledge about the mechanical properties of the different tissue layers. A non-invasive technique for estimation of the spatial variation of elasticity is ultrasound elastography. Ultrasound elastography measures tissue strain, from which the elastic properties can be deduced [13], [14], [15]. FE models of tissue displacements also require an accurate description of geometry and boundary conditions, as these

This research was supported by funds from the Netherlands Organization for Scientific Research (NWO). The authors thank Youri R. J. van Veen and Gerben te Riet o/g Scholten for their technical support.

J. op den Buijs, M. Abayazid, and S. Misra are with MIRA–Institute of Biomedical Technology and Technical Medicine (Control Engineering Group), University of Twente, The Netherlands. s.misra@utwente.nl

C. L. de Korte is with the Department of Pediatrics (Clinical Physics Laboratory), Radboud University Nijmegen Medical Centre, The Netherlands.

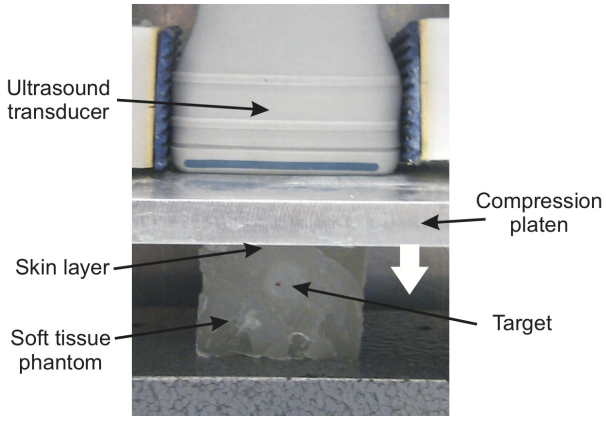

Fig. 2. Setup for ultrasound elastography measurements to obtain elastic moduli for input into the FE model.

factors have been shown to dominate target motion [16]. Changes in boundary conditions could be caused by patient motion, or the presence or absence of surrounding anatomical constraints, such as bone structures or connective tissue.

The hypothesis of this study was that with *a priori* knowledge about geometry and boundary conditions, and an approximate estimate of elasticity, target motion upon indentation of breast soft tissue phantoms can be accurately predicted with FE models. To test this hypothesis,

1) We modeled tissue indentation of inhomogeneous breast soft tissue phantoms using three-dimensional (3D) FE models.
2) A non-invasive estimation of the elasticity in the phantoms was obtained by ultrasound elastography.
3) The models were experimentally validated by ultrasound measurements of target motion during indentation of gel phantoms.
4) The influence of geometry and boundary conditions was investigated by modeling and testing both cubic and hemispherical phantoms, and by changing the boundary conditions for the cubic phantom.

After development and experimental validation of the FE model, we used it to explore the influence of various model parameters on target motion. These parameters included skin thickness and elastic modulus, target depth, diameter and elastic modulus, and indentor/target alignment.

This paper is organized as follows: Section II outlines the experiments used to validate the FE models. It describes the manufacturing of breast soft tissue phantoms, the experimental setup used for indentation, and the tracking of target displacements with ultrasound. Section III describes the development of the FE models used to simulate phantom indentation. Section IV summarizes the experimental results. Comparison of the experimental results to the FE predictions, along with FE-based sensitivity analysis are presented in Section V. Discussion of the results and study limitations are given in Section VI, followed by conclusions.

II. Experimental Methods

A. Breast soft tissue phantom preparation

Breast soft tissue phantoms were manufactured consisting of a gel to mimic adipose tissue, a stiff target to represent a lump, and a layer of silicone rubber to mimic skin. A mixture of 8.0%-by-weight gelatin (Dr. Oetker, Ede, The Netherlands), and 1.0%-by-weight silica gel (particle size < 63 μm SiC, E. Merck, Darmstadt, Germany) was added to boiling water and stirred. The silica gel served to mimic tissue acoustic scattering. The solution was then poured into a mold. To investigate the effect of geometry, we used molds that produced cubic phantoms ($40\times40\times40$ mm^3) and hemispherical phantoms (100 mm diameter). The stiff target was made from a small bead of silicone rubber of about 8.0 mm diameter. The rubber bead was positioned in the gel using a thin wire. After solidification of the gel for about one hour at 7°C, the thin wire was removed. A layer of silicone rubber with a thickness of approximately 1.5 mm was then deposited onto the phantoms, to represent the skin layer. The rubber layer was allowed to solidify for about one hour at room temperature. The phantom was allowed to solidify further at 7°C for several days before experimental testing.

B. Non-invasive determination of elastic modulus

To measure the relative elastic modulus between the skin layer and the stiff target, and the gel of the phantom, we used ultrasound elastography. The cubic breast tissue phantom was placed between the rigid platens of a compression setup, of which the top platen could be translated vertically using a manual micrometer. Radio-frequency (RF) two-dimensional (2D) ultrasound data were recorded with a SONOS 7500 real-time system (Philips Medical Systems, Best, The Netherlands), equipped with a linear array transducer (L11-3) with a central frequency of 7.5 MHz (Figure 2). RF-data were sampled at 39 MHz and were acquired in the unstressed state, and after applying compressive axial displacements in five steps of 1.2 mm to the top face of the phantom. Hence, a total displacement of 6.0 mm (15% strain for a cube of height 40 mm) was applied. A previously published method was used to estimate displacements and strains [15] by cross-correlation of two sequential RF-data sets. This algorithm used a coarse-to-fine cross-correlation algorithm with subsample resolution to determine the axial displacement field. Axial strains were then calculated using a least-squares strain estimator [17]. Calculations were performed in MATLAB (The Mathworks Inc., Natick, USA).

A plane-stress variant of a previously published inverse FE method [18] was used to reconstruct the distribution of elastic moduli from the strain images. A 2D plane-stress FE model consisting of 120×120 linear quadrilateral elements with 0.25 mm edge length was constructed. The algorithm was initialized with a homogeneous distribution of the relative Young's modulus $E = 1$ at iteration $i = 0$ to obtain an initial prediction of stresses and strains. The Young's moduli were then computed by iteratively calculating the Young's moduli according to

$$E^{i+1} = \frac{\sigma_y^i - \nu\sigma_x^i}{\varepsilon_y^{data}}, \qquad (1)$$

where σ_x^i and σ_y^i are the lateral and axial stress components, respectively. The axial strain ε_y^{data} was obtained by linear interpolation of the ultrasound strain data onto the nodes of the FE mesh.

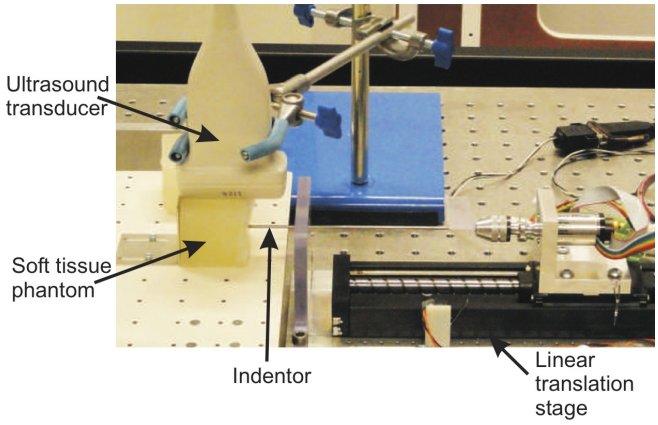

Fig. 3. Photograph of the breast phantom indentation setup. A linear array ultrasound transducer is mounted on top of a soft tissue phantom.

C. Experimental setup

A photograph of the setup is shown in Figure 3. The indentation of the soft tissue phantom was performed by placing a 2.0 mm diameter stainless steel indentor with blunt tip into a subassembly mounted on a linear translation stage (Misumi Group Inc., Tokyo, Japan). The linear stage was actuated via a DC motor with planetary gearhead with transmission ratio of 4.4:1 and optical encoder (Maxon Motor AG, Sachseln, Switzerland), which was operated by a controller (Elmo Motion Control Ltd., Petach-Tikva, Israel). The indentor was positioned such that it was just touching the skin layer of the phantom. The indentor was then moved forward with a velocity of 2.0 mm/s to indentation distances of 2.0, 4.0, and 6.0 mm. After each indentation, the indentor was returned to its original position. B-mode ultrasound images of the target were recorded for 4 seconds at 32 frames per second by a Philips HD 11XE ultrasound system (Philips Medical Systems, Best, The Netherlands), equipped with a linear array ultrasound transducer (L12-5). The transducer was positioned on top of the phantom with a clamp, such that the stiff target was in the field of view. Ultrasound measurements were recorded for three experimental cases:

- Case 1: The indentor was positioned horizontally with the tip touching the middle of the skin layer (Figure 4A).
- Case 2: The back support was partially removed, to simulate a change in boundary conditions, such as the absence of anatomical constraints. The indentor was positioned horizontally with the tip touching the middle of the skin layer (Figure 4B).
- Case 3: The hemispherical phantom was used. The indentor was positioned horizontally at a height of 20 mm (Figure 4C).

For each case, $n = 3$ experiments were performed on the same phantom.

D. Target motion tracking

Ultrasound images with 0.09×0.09 mm pixels were exported from the ultrasound system in DICOM format and imported into Matlab (The Mathworks Inc., Natick, USA). A digital image correlation (DIC) algorithm was used to track the displacement of a set of 8 pixels on the target/tissue boundary. The DIC algorithm used 2D cross-correlation of a square of 15×15 pixels around pixel

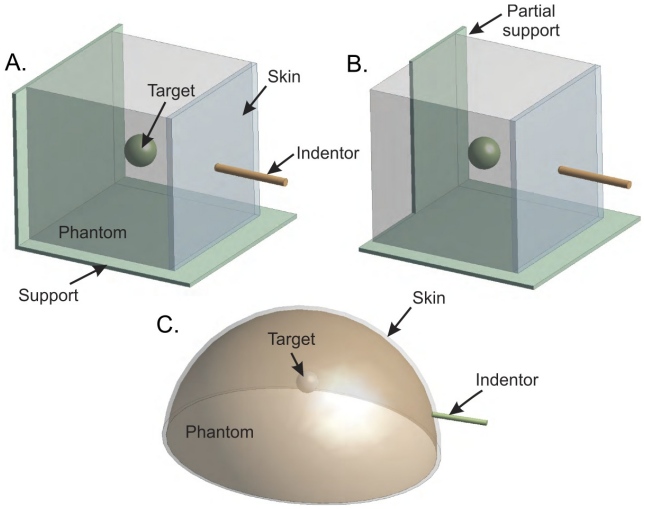

Fig. 4. Schematic of indentation experiments. **A.** Case 1: The side of the cubic phantom with the skin layer was indented in the middle. **B.** Case 2: The support of the back side of the phantom was partially removed. **C.** Case 3: The effect of a curved surface was investigated by indentation of a hemispherical phantom.

coordinates (x_k, y_k) in frame k with a square of 30×30 pixels in frame $k + \Delta k$. The peak location of the correlation values was detected by parabolic interpolation, resulting in determination of $(x_{k+\Delta k}, y_{k+\Delta k})$ with sub-pixel resolution. Steps of $\Delta k = 2$ frames were used. The target motion (u_k, v_k) was calculated as $(x_k - x_0, y_k - y_0)$, with the total displacement $U_k = \sqrt{u_k^2 + v_k^2}$. The average of the set of 8 pixels was reported as the total target displacement.

III. Finite Element Model: Phantom Indentation

A. Model description

To predict the target motion during the indentation of the surface of the breast tissue phantom, a 3D FE model was constructed and boundary conditions were applied to mimic the three experimental cases. The FE model was defined by the equilibrium equation, the strain-displacement relation, and a constitutive material model. In the absence of body forces, the equilibrium equation was given by

$$\nabla \cdot \boldsymbol{\sigma} = 0, \tag{2}$$

where $\boldsymbol{\sigma}$ is the stress tensor. The breast soft tissue phantom materials were modeled as linear isotropic elastic media with the constitutive equation given by

$$\boldsymbol{\sigma} = \frac{E}{1+\nu}\boldsymbol{\varepsilon} + \frac{E\nu}{(1+\nu)(1-2\nu)}\mathrm{tr}(\boldsymbol{\varepsilon})\mathbf{I}, \tag{3}$$

where $\boldsymbol{\varepsilon}$ is the strain tensor, tr is the trace operator, $\mathbf{I}$ is the second-order identity tensor, E is the Young's modulus, and ν is the Poisson's ratio. Strains are related to the displacements via

$$\boldsymbol{\varepsilon} = \frac{1}{2}\left[\nabla \mathbf{u} + (\nabla \mathbf{u})^T\right], \tag{4}$$

where $\mathbf{u}$ are the displacements.

The indentor was incorporated in the FE model, to account for the nonlinear contact conditions between indentor and tissue phantom. We assumed frictional contact, with a coefficient of friction of 0.1.

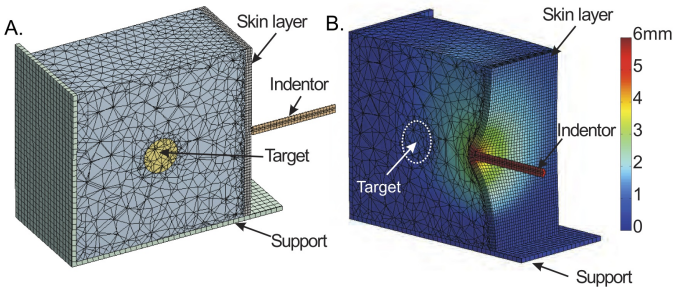

Fig. 5. **A.** Meshes with approximately 60,000 elements were considered converged for prediction of target displacements. A section plane through the stiff target is shown. Hexahedral elements were used for the indentor, skin layer and support. Tetrahedral elements were used for the phantom and target. **B.** Total displacement field in the cubic phantom upon 6.0 mm indentation.

TABLE I

LIST OF PARAMETER VALUES USED IN THE SENSITIVITY ANALYSIS.

Model parameter	Baseline value	Sensitivity
Skin thickness	1.5 mm	(1.0 mm, 2.0 mm)
Skin elastic modulus	0.5 MPa	(0.05 MPa, 5.0 MPa)
Target elastic modulus	0.5 MPa	(0.05 MPa, 5.0 MPa)
Target diameter	8.0 mm	(0.6 mm, 1.0 mm)
Target depth	20 mm	(15 mm, 25 mm)
Indentor/target alignment	Centered	(2.5 mm, 5.0 mm)

The FE mesh consisted of second-order hexahedral elements for the support and skin layer, and second-order tetrahedral elements for the remainder of the phantom and the indentor (Figure 5). To ease convergence of the nonlinear contact conditions, quasi-static simulations were carried out, such that the indentation depth was ramped up from 0 to 6.0 mm in 20 substeps. The FE calculations were performed with the commercial software ANSYS Workbench (ANSYS Inc., Canonsburgh, USA). Computations were executed on an eight-core 64-bit Intel Xeon workstation with 12 GByte internal memory.

B. Sensitivity analysis

To determine which parameters had the most effect on target motion during indentation, a sensitivity study was carried out with the indentation model using the cubic phantom with full support as a baseline. The model parameters were varied around a baseline value as listed in Table I, and the total target motion upon 6.0 mm indentation was computed by the FE model. While varying one model parameter, other parameters where kept at their baseline values. Using this approach, we calculated the sensitivity of target motion to thickness of the skin layer, skin elastic modulus, and target elastic modulus, size and depth. In addition, we carried out simulations where the indentor was translated in the horizontal plane, to simulate misalignment between the indentor and the target. Parameters that were not part of the sensitivity analysis included the Poisson's ratio, which was assumed equal to 0.3 for all materials. Elastic modulus of the gel (i.e., simulant for adipose tissue) was set to 10 kPa. The diameter of the indentor was 2.0 mm with a blunt tip.

IV. EXPERIMENTAL RESULTS

A. Non-invasive estimation of material properties

Ultrasound elastography (Figure 6A) clearly revealed the lower axial strain magnitude in the target and skin layer,

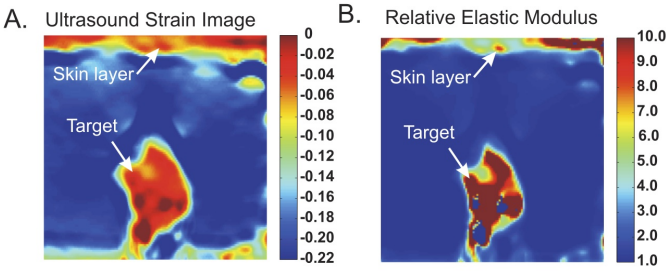

Fig. 6. Ultrasound elastography was used to obtain elastic moduli for input into the FE model. **A**. Axial strain image obtained from ultrasound elastography. **B**. Relative elastic modulus distribution calculated from the strain image using the inverse FE approach described in section II-B.

as compared to the surrounding material. The compressive axial strain was -0.03 in the target and -0.22 in the surrounding gel. The plane stress inverse FE method, described in Section II-B, was used to calculate relative Young's moduli (Figure 6B). After ten iterations, the Young's modulus distribution converged. The elastic modulus of the target and skin layer was found to be 17.6 times higher than the elastic modulus of the surrounding gel.

B. Ultrasound tracking of target motion

Representative B-mode ultrasound images of the target before and after 6.0 mm indentation of the cubic phantom reveal slight motion of the target. Even though the target only moves about 6 to 7 pixels (resolution 0.09 mm) during an indentation of the phantom surface by 6.0 mm, we used the 2D cross-correlation technique described in Section II-D, which allowed calculation of the total displacement of the target with subpixel resolution. As expected, increasing the indentation depth resulted in increased target displacement (Figure 7).

V. FINITE ELEMENT MODEL PREDICTIONS

A. Comparison of ultrasound measurements and finite element model

Target motions upon increased indentation were compared for the three experimental cases with FE models (Figure 8). For the cubic phantom, measured target displacements were compared to FE predictions for the cases where the back side of the phantom was fully supported and partially supported, as explained in Section II-C. As expected, this revealed

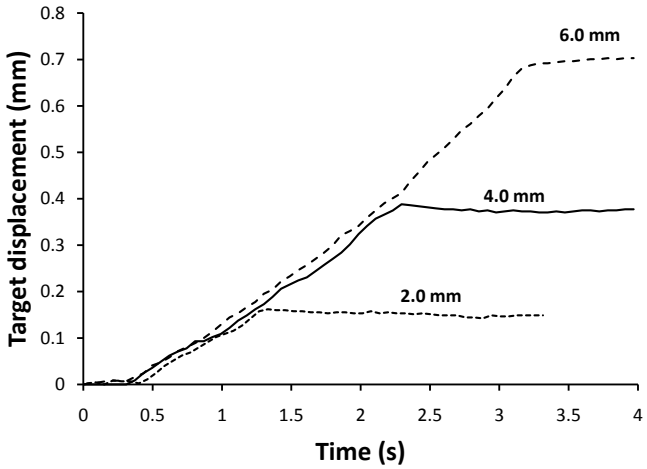

Fig. 7. Target displacement as a function of time for the cubic phantom (Case 1). Target displacement is shown for 2.0, 4.0 and 6.0 mm indentation.

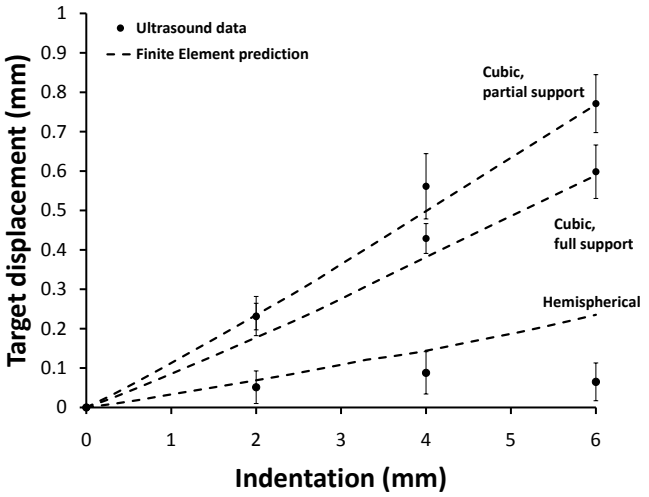

Fig. 8. Comparison of FE predictions of target motion (dashed lines) to ultrasound measured target motion (dots with error bars, $n = 3$ experiments). Comparisons are shown for the cubic phantom with full and partial support, and for the hemispherical phantom. Note that at 6.0 mm indentation of the hemispherical phantom, rupture of the phantom caused a decrease in target displacement.

that target motion was larger in the case of the partially supported phantom. The FE model accurately predicted the experimentally measured target motions, and also predicted a larger displacement in the case of partial support. The error between measured and predicted target displacement was 0.01 mm (12%) for the cubic phantom with full support and 0.002 mm (3%) for the cubic phantom with partial support.

Target motions measured by ultrasound were lower in the hemispherical phantom as compared to the cubic phantom, most likely due to the increased target depth. Furthermore, we measured a decrease in target motion from 4.0 to 6.0 mm indentation. This likely occurred as a result of rupture of the phantom skin layer and/or gel. The FE model also predicted a lower target motion, but overestimated the measured target motions. The error between predicted and measured target motion was 0.19 mm (79%) upon 6.0 mm indentation. Since the FE model did not incorporate a damage model, rupture of the tissue could not be predicted, which may have resulted in the observed overestimation of target motion at 6.0 mm indentation of the hemispherical phantom.

B. Parameter sensitivity study

The FE model of the cubic phantom was used to explore the influence of various parameters on target motion. The results of this sensitivity study suggested that the elastic modulus of the skin layer had a large effect on target motion during indentation. Upon increasing the skin elastic modulus from 0.5 to 5.0 MPa, target motion increased by 239% (Figure 9A). Also skin thickness had a moderate effect on target motion (Figure 9B). Increasing skin thickness from 1.0 to 2.0 mm increased target motion by 54%. Target elastic modulus did not have a large effect on target motion (Figure 9C). Decreasing target depth considerably increased target motion, as expected (Figure 9D). An increase in target motion by 131% was calculated when decreasing target depth from 25 to 15 mm. On the other hand, target diameter (Figure 9E) and indentor/target alignment (Figure 9F) did not have a great influence on predicted target motion.

VI. Discussion

Pre-operative planning in combination with robotic needle insertion holds the promise to improve targeting accuracy during breast biopsies and other percutaneous needle insertion procedures [19]. We used ultrasound elastography to obtain an estimate of the distribution of elasticity in a breast tissue phantom. These properties were used in an FE model to predict target displacements upon indentation of the phantom surface layer. To validate the model, a robotic needle insertion setup was used to perform indentation experiments on a breast tissue phantom. Ultrasound measurements were carried out to track the target during indentation. Comparison between FE predictions and measurements confirm our hypothesis that with *a priori* knowledge about geometry and boundary conditions, and an approximate estimate of elasticity, target motion upon indentation of breast soft tissue phantoms can be accurately predicted with FE models.

Using FE sensitivity studies, we investigated the influence of geometrical and mechanical properties on target motion upon indentation of the breast phantom. This study predicted that target motion is greatly influenced by skin elastic modulus and target depth, whereas the influence of target elastic modulus and size on target motion is minimal. Hence, accurate measures of skin elastic modulus and target depth should be obtained for pre-operative planning of breast biopsies.

Breast tissue phantom indentation was investigated because it was expected that indentation has the most influence on target motion during insertion of a needle. However, the maximum amount of indentation is determined by the moment of rupture of the tissue. As a preliminary study, we have modeled needle insertion by deleting elements from the FE mesh when a strain limit in these elements is exceeded. The results of this preliminary experiment were compared with ultrasound measurements (Figure 10). The maximum target motion measured with ultrasound was 2.0 mm, whereas the FE model predicted a maximum target motion of 2.1 mm during the insertion. These preliminary results demonstrate the feasibility of using explicit dynamics and element deletion to model needle insertions, and we will use this method in future work to predict target displacements upon needle insertion.

Ultrasound displacement measurements were performed using a linear array transducer, and out-of-plane displacements were not available. However, out-of-plane motions may not have been negligible in some of our experimental scenarios, and will most definitely have an influence in heterogeneous tissues. Since 3D ultrasound imaging is available, and progress has been made towards the estimation of 3D displacement fields from ultrasound data [20], it is likely that the FE models can be validated with 3D data in the near future.

A. Conclusions

FE models can be used to predict target motions for indentation of breast tissue phantoms. Our FE model predictions agreed well with ultrasound measurements of target displacements in cubic phantoms. Predictions of target motion in hemispherical phantoms still require improvement. Parameter sensitivity analysis of the FE model showed that skin

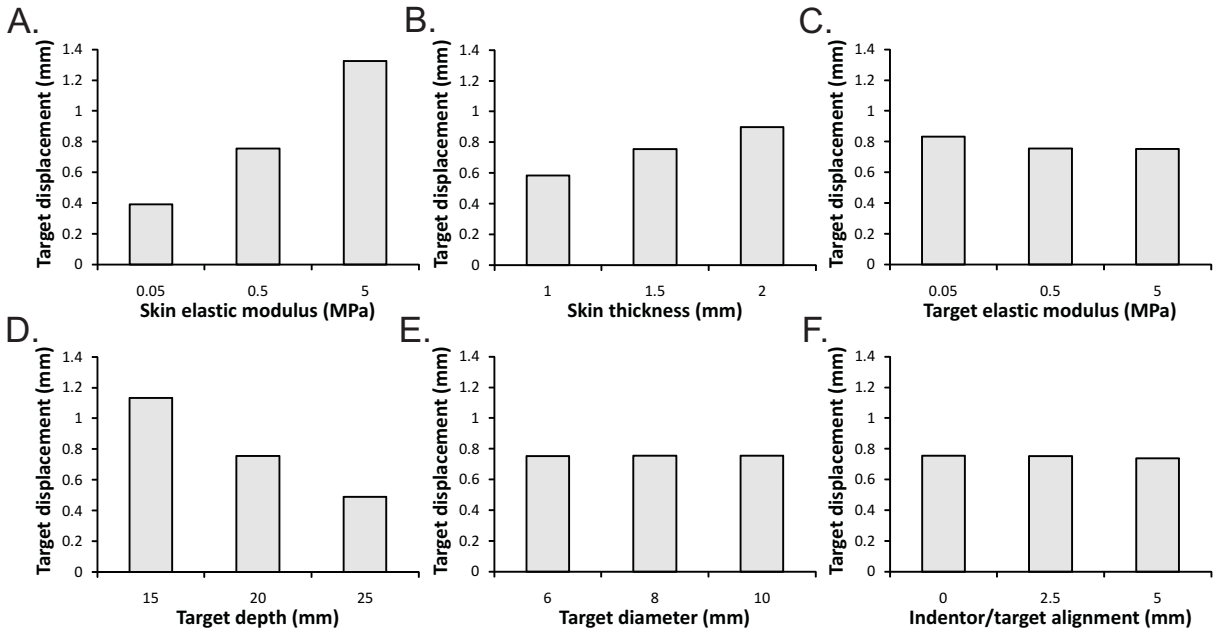

Fig. 9. FE predicted influence on target motion of: **A.** Skin elastic modulus. **B.** Skin thickness. **C.** Target elastic modulus. **D.** Target depth. **E.** Target diameter. **F.** Indentor/target alignment.

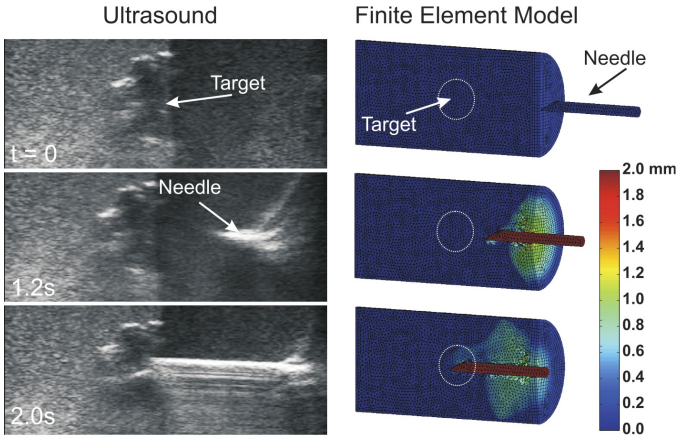

Fig. 10. Time series of ultrasound images compared with FE simulations during insertion of a 2.0 mm diameter needle with 30° bevel angle to a 20 mm depth into the cubic breast tissue phantom. Color scale in the FE simulations represents deformation in mm.

elastic modulus and target depth are important parameters in predicting target motion. Furthermore, *a priori* knowledge of organ geometry and surrounding boundary conditions should be accurately taken into account during the pre-operative planning phase, as it dominates target motion.

REFERENCES

[1] "Breast cancer statistics", *www.breastcancer.org*, 2010.

[2] Kaiser *et al.*, "MRI-guided interventions of the breast", *Journal of Magnetic Resonance Imaging*, vol. 27, no. 2, pp. 347–355, 2008.

[3] Schueller *et al.*, "Accuracy of ultrasound-guided, large-core needle breast biopsy", *European Radiology*, vol. 18, no. 9, pp. 1761–1773, 2008.

[4] R. G. Stock and N. N. Stone, "Current topics in the treatment of prostate cancer with low-dose-rate brachytherapy", *Urologic Clinics of North America*, vol. 37, no. 1, pp. 83–96, 2010.

[5] Abolhassani *et al.*, "Needle insertion into soft tissue: a survey", *Medical Engineering and Physics*, vol. 29, no. 4, pp. 413–431, 2007.

[6] Deurloo *et al.*, "Displacement of breast tissue and needle deviations during stereotactic procedures," *Investigative Radiology*, vol. 36, no. 6, pp. 347–353, 2001.

[7] Abolhassani *et al.*, "Minimization of needle deflection in robotassisted percutaneous therapy", *International Journal of Medical Robotics and Computer Assisted Surgery*, vol. 3, no. 2, pp. 140–148, 2007.

[8] Fichtinger *et al.*, "Robotic assistance for ultrasound guided prostate brachytherapy", in *Proccedings of the Med- ical Image Computing and Computer-Assisted Intervention (MICCAI) Conference*, vol. 4791, no. 1, pp. 119–127, Brisbane, Australia, October-November 2007.

[9] Misra *et al.*, "Modeling of tool-tissue interactions for computer-based surgical simulation: a literature review", *Presence: Teleoperators and Virtual Enviornments*, vol. 17, no. 5, pp. 463–491, 2008.

[10] S. P. DiMaio and S. E. Salcudean, "Interactive simulation of needle insertion models", *IEEE Transactions on Biomedical Engineering*, vol. 52, no. 7, pp. 1167–1179, 2005.

[11] Barbé *et al.*, "Needle insertions modeling: identifiability and limitations," *Biomedical Signal Processing and Control*, vol. 2, no. 3, pp. 191–198, 2007.

[12] Dehghan *et al.*, "Needle-tissue interaction modeling using ultrasound-based motion estimation: phantom study", *Computer Aided Surgery*, vol. 13, no. 5, pages 265-280, 2008.

[13] Ophir *et al.*, "Elastography: a quantitative method for imaging the elasticity of biological tissues", *Ultrasonic Imaging*, vol. 13, no. 2, pp. 111–134, 1991.

[14] De Korte *et al.*, "Intravascular elasticity imaging using ultrasound: feasibility studies in phantoms", *Ultrasound in Medicine and Biology*, vol. 23, no. 5, pp. 735–746, 1997.

[15] Lopata *et al.*, "Performance evaluation of methods for two-dimensional displacement and strain estimation using ultrasound radio frequency data", *Ultrasound in Medicine and Biology*, vol. 35, no. 5, pp. 796–812, 2009.

[16] Misra *et al.*, "The importance of organ geometry and boundary constraints for planning of medical interventions", *Medical Engineering and Physics*, vol. 31, no. 2, pp. 195–206, 2009.

[17] Lopata *et al.*, "Comparison of one-dimensional and two-dimensional least-squares strain estimators for phased array displacement data", *Ultrasonic Imaging*, vol. 31, no. 1, pp. 1–16, 2009.

[18] M. Yamakawa and T. Shiina, "Tissue elasticity reconstruction based on 3-dimensional finite-element model", *Japanese Journal of Applied Physics*, vol. 38 part 1, no. 5B, pp. 3393–3398, 1999.

[19] Alterovitz *et al.*, "Sensorless motion planning for medical needle insertion in deformable tissues", *IEEE Transactions on Information Technology in Biomedicine*, vol. 13, no. 2, pp. 217–225, 2009.

[20] Richards *et al.*, "Quantitative three-dimensional elasticity imaging from quasi-static deformation: a phantom study", *Physics in Medicine and Biology*, vol. 54, no. 3, pp. 757–779, 2009.